Moving bed temperature swing adsorption for CO_2 capture from a natural gas combined cycle power plant

Giorgia Mondino[a,*], Carlos A. Grande[b], Richard Blom[b], Lars O. Nord[a]

[a] *NTNU - Norwegian University of Science and Technology, Department of Energy and Process Engineering, Trondheim, Norway*
[b] *SINTEF Industry, P.O. Box 124 Blindern, N0314 Oslo, Norway*

Abstract

The present work considers the utilization of a Moving Bed Temperature Swing Adsorption (MBTSA) process for CO_2 capture as alternative to the commercial absorption-based technologies, in the context of Natural Gas Combined Cycle (NGCC) power plants. A detailed mathematical model consisting of energy, mass and momentum balances was implemented in gPROMS software, in order to investigate the system behavior under different operating conditions and design parameters. Results show that under the simulated process conditions, the system is suitable for capturing CO_2 at high purity and high capture rate. Promising results are obtained also in terms of process energy duty, by performing a preliminary analysis that takes into account the heat required for sorbent regeneration. Furthermore, the effect of implementing the MBTSA process on plant performance was studied, by integrating the capture system with a process model of the reference power plant. A detailed analysis of the energy use associated with the capture process auxiliaries was performed. Finally, the power plant model was used to simulate the same NGCC system coupled with a state-of-the-art absorption process, for a direct comparison between the two capture technologies.

Keywords: TSA, MBTSA, NGCC, post-combustion, PCC, CCS, Zeolite 13X

1. Introduction

In post-combustion CO_2 capture, adsorption processes are considered a promising alternative to the commercial absorption-based technology, which suffers from high costs and high energy penalties (Liang et al., 2016). While requiring further developments as a CO_2 capture technology, solid sorbents are already commercially used in a wide range of applications, from air separation, to hydrogen purification, gas drying and methane purification (Ruthven, 1984). In all these processes, the adsorbent material is used in a cyclic manner, switching between adsorption and desorption steps, where the latter (i.e. sorbent regeneration) is performed either by a change in pressure (Pressure Swing/Vacuum Pressure Swing)

*Corresponding author
Email address: giorgia.mondino@ntnu.no (Giorgia Mondino)

or in temperature (Temperature Swing). The same concept can be employed for post-combustion CO_2 capture, provided that the adsorbent is selective toward CO_2 at the flue gas conditions.

The main issue with conventional temperature swing adsorption (TSA) processes, where the adsorbent is packed in large columns, is the long cycle time associated to the heating and cooling steps, which can take several hours (Plaza et al., 2017) . One way to overcome this issue, thus significantly improving the efficiency of the separation process, is to employ the moving bed temperature swing adsorption (MBTSA) concept, in which the adsorbent circulates through different sections, always operated at the same conditions for their specific purpose: adsorption, desorption, or cooling.

The MBTSA process has been previously suggested for CO_2 capture by Knaebel (Knaebel, 2009) and SRI International (Hornbostel et al., 2013), who respectively used zeolites and activated carbons as adsorbent materials. The same concept has been lately proposed as a viable option for post-combustion capture by Kim et al. (Kim et al., 2013, 2014, Son et al., 2014), who investigate the possibility of reducing the energy penalty of the process by internal heat integration.

At GHGT-13 we presented a simplified assessment of the MBTSA process in the Natural Gas Combined Cycle (NGCC) context (Grande et al., 2017). More recently we have carried out a more comprehensive study of the MBTSA process using the composite model approach in gPROMS software (gPROMS Model Builder Version 5.0) to simultaneously simulate the different sections composing the MBTSA (Mondino et al., 2017). The composite model was used to investigate the application of the MBTSA for CO_2 from a coal fired power plant. Based on the detailed model for the coal case (Mondino et al., 2017), the present work aims to give a more thorough assessment of the performance of an MBTSA process in the NGCC context. For this purpose, the configuration of the system is adapted to the NGCC case study, which differs from the coal fired power plant in terms of flue gas conditions (temperature, pressure, flow rate and composition). Due to the lower CO_2 partial pressure in the flue gas, the use of zeolites is considered, as zeolites present a significantly higher selectivity towards CO_2 compared to activated carbons (Chue et al., 1995).

Adsorption equilibrium data was experimentally measured for the selected adsorbent and fitted with a mathematical model in order to provide the required model parameters. A set of simulations was performed by varying several design parameters and operating conditions, as well as adjusting the system configuration, in order to reach the desired product gas specifications, in terms of CO_2 purity and capture rate. Furthermore, the amount of energy required for sorbent regeneration was evaluated by applying the energy balance across the preheating and desorption sections of the moving bed, where the adsorbent was heated to the regeneration temperature. The use of steam from the power plant was considered for this purpose, in addition to a heat integration scheme that reduces the need of external heat by recovering heat within the MBTSA system.

In order to evaluate the impact of the CO_2 capture system on the power plant efficiency, Thermoflex software was used (Thermoflow Version 27). A computational model of the NGCC power plant able to accommodate the capture system was built, and full plant-analysis performed. The power plant model was also used to simulate the same NGCC

system without CO_2 capture unit, as reference case, as well as a NGCC system coupled with a state-of-the-art absorption process, for a direct comparison between the two capture technologies.

2. Framework for the process simulations

The application considered for the MBTSA capture process consists of an NGCC with a net power output of nearly 800 MW. The power plant was initially modelled through GT PRO software (Thermoflow package (Thermoflow Version 27)), in order to provide the input data for the MBTSA model, in terms of flue gas specifications.

The NGCC object of this study was designed with the aim of representing the current state-of-the-art technology in combined cycles, which are engineered to achieve net efficiencies exceeding 63 % LHV based (Vandervort, 2018). For this purpose, the General Electric 9HA.02 model was adopted for the Gas Turbine (GT), fueled by natural gas. Details on the natural gas compositions and heating values are listed in Appendix A.

A three pressure levels and reheat type steam cycle configuration was employed. As a common measure to increase the power plant efficiency (Fernandez et al., 2014, Anantharaman et al., 2011), the fuel is preheated prior the combustor with part of the steam produced in the intermediate pressure (IP) drum. The resulting plant layout is shown in Figure 1, while a summary of the main operating conditions and performance parameters is presented in Table 1.

The next paragraphs contain a description of the MBTSA process and model approach, followed by a description of the adsorbent material employed and characterized. Furthermore, details are given on how the MBTSA model results were used as basis for the integration of the capture process with the power plant for full-plant analysis. Finally, some details are given concerning the comparison of the MBTSA process with an amine-based CO_2 capture process.

2.1. The MBTSA process and model simulations

A schematic diagram of an MBTSA system is shown in Figure 2. As shown in the figure, the MBTSA system is composed of the following three main sections through which the pelletized adsorbent circulates: the adsorption section at the top (black in the figure), the desorption section (red in the figure) and the cooling section at the bottom (blue in the figure).

In the adsorption section the adsorbent particles falls counter-currently to the flue gas, capturing the incoming CO_2. The adsorbent leaving from the bottom of the adsorption section is loaded with CO_2 extracted from the flue gas and continues into the desorption (regeneration) section. In the desorption section, heat is transferred to the adsorbent promoting desorption of CO_2 that is further assisted by light vacuum for extraction. In this work it is assumed that the desorption section is operated as an indirect-contact heat exchanger where steam from the power plant is used as heat transfer fluid.

The unloaded adsorbent is then cooled down in the cooling section and transported back to the top of the reactor, ready to start a new cycle. As shown in the figure, preheating

Table 1: Summary of technical data of the reference NGCC plant.

Gas cycle	
GT model	GE 9HA.02
Fuel type	Natural gas
Net fuel energy input (MW)	1257.3
GT gross electric power output (MW)	555.3
Fuel temperature at combustor inlet (°C)	180
Fuel pressure at combustor inlet (bar)	39.29
Fuel flow (kg/s)	27.17
Air temperature at compressor inlet (°C)	15
Air flow (kg/s)	957
GT inlet temperature (°C)	1504.5
GT exhaust temperature (°C)	646.9
GT exhaust pressure (bar)	1.051 bar
GT exhaust gas flow (kg/s)	984.1
Steam cycle	
Number of pressure levels	3
ST gross electric power output (MW)	246.5
HP turbine inlet temperature (°C)	600
HP turbine pressure (bar)	186
HP turbine inlet flow (kg/s)	126
IP turbine inlet temperature (°C)	600
IP turbine inlet pressure (bar)	30
IP turbine inlet flow (kg/s)	142.9
LP turbine inlet temperature (°C)	72.32
LP turbine pressure (bar)	0.3447
LP turbine inlet flow (kg/s)	161
Condenser pressure (bar)	0.0586
Combined cycle	
Gross combined electric power output (MW)	801.8
Net power output (MW)	792.8
Net electric efficiency	63.05
CO_2 emitted (kg/s)	70.82

and precooling sections can also be employed in order to recover part of the heat from the hot powder leaving the desorption section for preheating the powder leaving the adsorption section.

The mathematical model describing the MBTSA (Figure 2) consists of a set of partial differential equations (unsteady and one dimensional) obtained by applying the mass, energy and momentum balance to the individual sections (adsorption, desorption and cooling section).

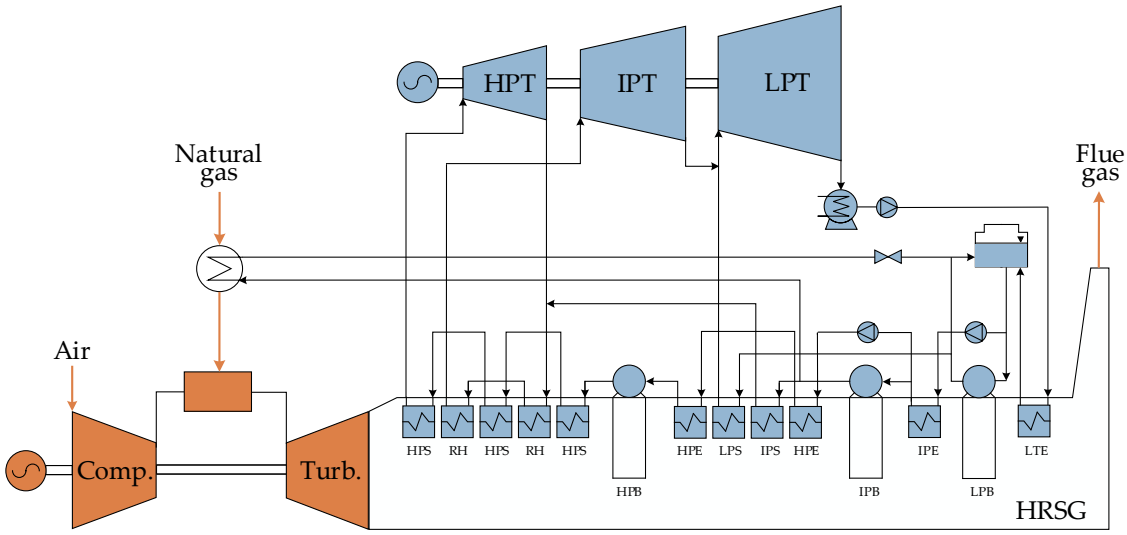

Figure 1: Layout of the reference NGCC power plant without CCS, where the following abbreviations are used: Comp. for compressor section in gas turbine, Turb. for turbine section in gas turbine, HPT, IPT and LPT for high, intermediate and low pressure steam turbines, respectively, HRSG for heat recovery steam generator, HPS, IPS, LPS for high, intermediate and low pressure superheaters, respectively, HPE, IPE, LPE for the corresponding economizers, HPB, IPB and LPB for the boilers, and RH for the reheater.

One of the main differences compared to a fixed-bed adsorption model is given by the terms containing v_{solid} (i.e. velocity of the solid) appearing in the mass and energy balance equations, which represent the contribution due to the movement of the adsorbent along the axial coordinate. It should be noted that, unlikely fixed bed adsorption systems, the counter current moving bed can be operated at steady state. Although a dynamic model is used for simulations, only the steady-state behaviours is investigated in this study, and all results presented were obtained during steady-state.

The set of coupled differential equations, implemented on gPROMS software for each section of the moving bed, has to be solved simultaneously for continuous process simulations. For this purpose, the individual units were connected to each other in a so-called "composite model" flowsheet on gPROMS (Liu et al., 2011). With the gPROMS composite model approach, the different sections of the moving bed communicate with each other through specifically defined variable-ports. The purpose of these inlet-outlet ports is to transfer certain model variables (e.g. gas and solid phase concentrations, temperature and pressure) at the boundary of the corresponding section-space domain, so that the model instances can exchange information with the adjacent model instances during simulation. As an example, the boundary conditions for the solid phase at the top of the adsorption section (i.e. sorbent inlet), will be assigned based on the variables computed within the cooling section, so that the conditions of the adsorbent leaving the cooling section are used as input at the top of the adsorption section. This allow to take into account for example for a non-complete regeneration of the solid performed in desorption section, which in turns

will affect the performance of the adsorption section, and thus the overall process. More details on the modelling approach and underlying assumptions can be found in Appendix B.

The simulations were performed by discretizing the axial space domain of each process sections with the Centered Finite Difference Method (CFDM), with second order approximation. The number of intervals employed to discretize the axial space domain was 200 for the adsorption and the cooling sections, 100 for the preheating and 400 for the desorption section.

A set of simulations was performed by varying several design parameters and operating conditions, as well as adjusting the system configuration, in order to improve the process performances, with the aim of obtaining high CO_2 purity and capture rate. The following values were set as minimum targets, based on the typical specifications required for CO_2 transport and storage: 95% CO_2 purity and 90% CO_2 capture rate.

Furthermore, the total amount of energy required for sorbent regeneration was evaluated by applying the energy balance across the preheating and desorption sections, where the adsorbent is heated to the regeneration temperature. The amount of thermal energy that can be recovered by transferring heat from the hot adsorbent leaving the desorption section to the adsorbent that has to be regenerated, was estimated by analyzing the temperature profiles along the heating and cooling sections, and the corresponding heat exchanged. A graphical procedure was used for this purpose, by plotting the hot and cold composite curves on an temperature-enthalpy diagram. The minimum amount of external heat required was estimated by moving the cold curve along the enthalpy axis so that a minimum temperature difference is ensured at the pinch point. As conservative assumption, considering that a third heat transfer media is used for transferring the recoverable heat, a value of 20 °C was assumed as ΔT minimum on both sides (hot and cold). With the same approach, the amount of external heat required was estimated in order to provide the input for process integration with the power plant.

As previously mentioned, the characteristics of the flue gas considered for the application of the MBTSA in this work refer to an NGCC power plant. In order to reduce the computational effort in the MBTSA simulations, the composition of the exhaust gas, obtained with the NGCC model in GT PRO software, was simplified to a binary mixture of N_2 and CO_2. For this purpose the following assumptions were made: O_2 and Ar behave similarly to N_2 (Baksh et al., 1992, Park et al., 2006, Merel et al., 2008), and the water vapor is removed prior the MBTSA unit. The resulting flue gas specifications, used as input for designing and simulating the MBTSA process, are listed in Table 2.

2.2. The adsorbent material

Besides reducing the computational effort of the MBTSA simulations, another reason for considering dried flue gas is to avoid limiting the choice of the adsorbent to those material having low affinity towards water, such as activated carbons. For the purpose of this study, it was therefore possible to employ a Zeolite 13X, which is suitable for the NGCC case, for its high CO_2 adsorption capacity at low CO_2 partial pressures and high CO_2/N_2 selectivity (Zanco et al., 2018, Hefti et al., 2015, Lillia et al., 2018, Merel et al., 2008).

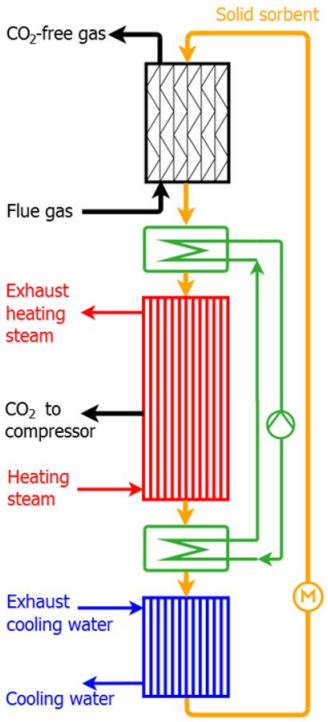

Mass balance in the gas phase

$$\varepsilon_c \frac{\partial C_i}{\partial t} = \varepsilon_c \frac{\partial}{\partial z}\left(D_z C_T \frac{\partial Y_i}{\partial z}\right) - \frac{\partial (u C_i)}{\partial z} - \frac{(1-\varepsilon_c-\xi)a' K_m}{Bi/5+1}(C_i - C_{b,i})$$

Mass balance in macropores of the adsorbent (LDF description)

$$\varepsilon_p \frac{\partial C_{b,i}}{\partial t} = \varepsilon_p \frac{15 D_{p,i}}{{R_p}^2} \frac{Bi_i}{5+Bi_i}(C_i - C_{b,i}) - \rho_p\left(\frac{\partial q_i}{\partial t} + v_{solid}\frac{\partial q_i}{\partial z}\right) - v_{solid}\frac{\partial C_{b,i}}{\partial z}$$

Mass balance in micropores of the adsorbent

$$\frac{\partial q_i}{\partial t} + v_{solid}\frac{\partial q_i}{\partial z} = \frac{15 D_{c,i}}{{r_c}^2}(q_i^* - q_i)$$

Adsorption isotherm (extension of Virial isotherm for multicomponent adsorption isotherm)

$$P_i = \frac{q_i^*}{K_i} exp\left[\sum_{j=1}^{N} A_{ij} q_j^* + \sum_{j=1}^{N}\sum_{k=1}^{N} B_{ijk} q_j^* q_k^* + \sum_{j=1}^{N}\sum_{k=1}^{N}\sum_{l=1}^{N} C_{ijkl}\, q_j^* q_k^* q_l^*\right] \qquad K_i = K_i^{\infty} exp\left(\frac{-\Delta H_i}{R_g T_s}\right)$$

$$A_i = A_{0,i} + \frac{A_{1,i}}{T_s}; \qquad A_{ij} = \frac{A_i + A_j}{2}; \qquad B_i = B_{0,i} + \frac{B_{1,i}}{T_s} \qquad B_{ijk} = \frac{B_i + B_j + B_k}{3}$$

Energy balance in the gas phase

$$\varepsilon_c C_T c_v \frac{\partial T}{\partial t} = \frac{\partial}{\partial z}\left(\lambda \frac{\partial T}{\partial z}\right) - u C_T c_p \frac{\partial T}{\partial z} + \varepsilon_c RT \sum \frac{\partial C}{\partial t} - (1-\varepsilon_c-\xi)a' h_f (T - T_s) - \frac{4\, h_{g,hx}}{D_h}(T - T_{hx})$$

Energy balance in the solid phase

$$\left[(1-\varepsilon_c-\xi)\rho_p c_{ps} + \xi \rho_{pack} c_{ppack}\right]\left(\frac{\partial T_s}{\partial t} + v_{solid}\frac{\partial T_s}{\partial z}\right) = \xi \frac{\partial}{\partial z}\left(\lambda_{pack}\frac{\partial T_s}{\partial z}\right) + (1-\varepsilon_c-\xi)a' h_f (T_g - T_s)$$
$$+(1-\varepsilon_c-\xi)\rho_p \sum\left(-\Delta H_i\left[\frac{\partial q_i}{\partial t} + v_{solid}\frac{\partial q_i}{\partial z}\right]\right) + (1-\varepsilon_c-\xi)\varepsilon_p RT_s \sum\left[\frac{\partial C_{b,i}}{\partial t} + v_{solid}\frac{\partial C_{b,i}}{\partial z}\right]$$

Figure 2: Schematic diagram of the MBTSA (right) and summary of model equations.

A sample of Zeolite 13X, pelletized into spherical particles of 700 μm diameter, was purchased by CWK, Germany. The size of the particles was chosen to be higher than few hundreds μm in order to avoid fluidization in the adsorption section of the moving bed, where large flow rates move counter currently to the adsorbent.

In order to provide the MBTSA model with the necessary data of the adsorbent, the purchased Zeolite 13X was characterized in terms of pure components adsorption isotherms of CO_2 and N_2. The measurements were performed in a volumetric apparatus (Belsorp Max, MicrotracBEL) at seven different temperatures in the range of 10 to 180 °C, up to 1.05 bar. Prior to the measurements the sample was regenerated at 320 °C under vacuum for 10 hours, in order to remove any presence of impurities or moisture adsorbed.

Fitting of the experimental data was performed using the Virial model (Taqvi and LeVan, 1997, Shen et al., 2012, Barrer, 1981), which provides the parameters to use as input for the multicomponent adsorption equations implemented in the MBTSA model. Details on the methods used for the isotherms fitting can be found elsewhere (Mondino et al., 2017). In order to account for competitive adsorption of the two gases, the extension of the Virial model for multicomponent adsorption equilibrium (Ribeiro et al., 2008, Shen et al., 2010) was implemented in the MBTSA simulations, as shown in Figure 2.

2.3. Integration of the MBTSA process and the power plant

In order to evaluate the impact of the CO_2 capture system on the power plant efficiency, the NGCC model initially developed in GT PRO was exported into Thermoflex and

Table 2: Main input parameters adopted in the MBTSA simulations: specifications of the NGCC exhaust gas and adsorbent properties.

Flue gas at MBTSA inlet	
Temperature	30 °C
Pressure	1.05 bar
Flowrate	916 kg/s
Composition:	
CO_2	5.15 vol%
N_2	94.85 vol%
Adsorbent properties	
Adsorbent type	Zeolite 13X
Particles shape	spheres
Paricles diameter	700 μm
Paricle porosity	0.5
Paricle density	1100 kg/m^3
Heat capacity	880 kJ/(kg K)

appositely modified in order to accommodate the capture process. The reason for using Thermoflex is that, compared to GT PRO, it allows a higher degree of model customization.

The layout of the NGCC power plant integrated with the MBTSA system is shown in Figure 3. The main modifications with respect to the reference case (NGCC plant without CO_2 capture, shown in Figure 1) include: (i) the extraction of steam from the IP turbine, needed in the MBTSA for sorbent regeneration, (ii) a drying unit, employed for removing water from the flue gas upstream the MBTSA, (iii) a compressor/fan compensating for the pressure drops of the MBTSA, (iv) a CO_2 compressor, (v) a cooling water circuit that takes into account the cooling demand of the MBTSA system.

The extracted steam is processed by an indirect counter current heat exchanger that mimics the desorption section of the MBTSA, in terms of inlet/outlet temperatures of the cold fluid and heat duty. The condensed water leaving the heat exchanger is returned to the deaerator after appropriate pressure reduction. The amount of steam extracted and the corresponding pressure will therefore be determined based on the heat exchanger duty, while assuring that the condensed outlet temperature corresponds to the deaerator operating temperature. A similar approach is used for simulating the cooling part of the MBTSA process, where cooling water is used, implying the use of a circulating pump.

The drying unit consists of three components: (i) a gas-water contact heat exchanger where the flue gas is cooled to 30 °C, (ii) an electric chiller that further reduces the temperature of the flue gas to 16 °C, (iii) a fan placed upstream the gas-water contact heat exchanger, for overcoming the pressure drops of the drying steps. The flue gas leaving the drying units still contains a small amount of water (approximately 1.8 mol%), which should also be removed. Although this final step was not included in the present work, it was assumed that the remaining water can be removed in a process with limited energy consumption, applying the same approach described by Lillia et al. (Lillia et al., 2018), where

the activated alumina used for adsorbing water is regenerated by the CO_2-free product of the capture process.

Lastly, the CO_2 compressor consists in five inter-cooled stages characterized by an isentropic efficiency of 85% for each stage. The inlet conditions (i.e. gas composition, flow rate, temperature and pressure) are set based on the results obtained with the MBTSA simulations. The delivery pressure is assumed to be 110 bar.

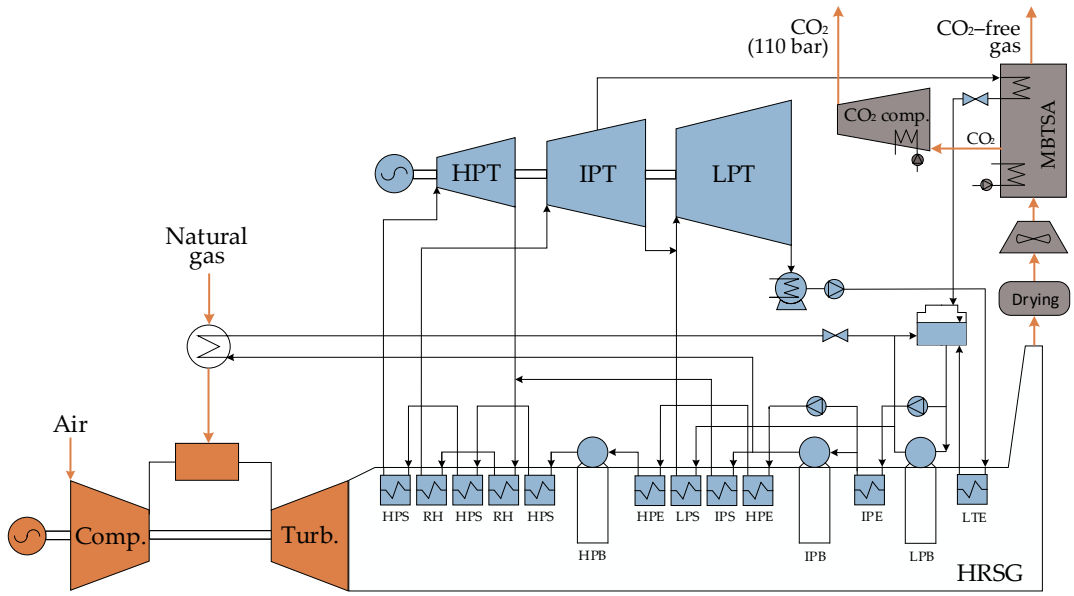

Figure 3: Layout of the reference NGCC power plant integrated with the MBTSA process. Comp. for air compressor, Turb. for gas turbine, HPT, IPT and LPT for high, intermediate and low pressure turbines, respectively, HRSG for heat recovery steam generator, HPS, IPS, LPS for high, intermediate and low pressure superheaters, respectively, HPE, IPE, LPE for the corresponding economizers, HPB, IPB and LPB for the boilers, and RH for the reheater

2.4. Comparison with an amine based capture process

One of the aims of this work is to provide a plant-level comparison of the developed MBTSA process with the benchmark amine based capture technology. For this purpose, the reference NGCC model was again modified in Thermoflex software (Thermoflow Version 27), which provides a built-in model of a standard chemical absorption process using MEA (MonoEthanolAmine) as solvent. Together with certain user-inputs, the built-in model provides an estimate of the total auxiliary power, heat consumption, and cooling duty required by the process, as well as its impact on the combined cycle efficiency.

The main input that were provided to the software when implementing this model are representative of a typical MEA process with a specific energy input of 3.95 MJ/kg (Fernandez et al., 2014, Franco et al., 2011, Anantharaman et al., 2011). A comprehensive list of process parameters adopted is can be found in Appendix A.

The implemented absorption process requires a certain amount of steam for covering the heat duty of the reboiler. Using the same approach used by Sanchez Fernandez et al. (Fernandez et al., 2014), the necessary steam is extracted at a pressure close to the steam condensing pressure in the reboiler and further conditioned for reboiler use. The condensate from the reboiler is pumped back to the feed water tank.

3. Results and discussion

3.1. Adsorption equilibrium of CO_2 and N_2 on Zeolite 13X

The results of CO_2 and N_2 isotherms measurements, performed on the Zeolite 13X in a wide range of temperature (10 to 180 °C), are shown in Figure 4, together with the isotherms fitting, given by the Virial model (solid lines). As expected, the adsorption capacity of CO_2 is significantly higher than the adsorption capacity of N_2, in the whole temperature and pressure ranges examined. At 30 °C and 0.0515 bar, which correspond the CO_2 partial pressure at the feed gas conditions, the equilibrium capacity of CO_2 is 3.5 mol/kg, versus 0.4 mol/kg of N_2 at the feed gas conditions (30 °C and 0.996 bar). This confirms the high equilibrium selectivity of the adsorbent, which is beneficial for the MBTSA process, where high purity of the CO_2 product is desired.

The values of the parameters obtained by fitting the isotherms with the Virial model are listed in Table 3. The heat of adsorptions obtained by the Virial fitting is in good agreement with the values obtained from the slope of the Van't Hoff plot, shown in Figure 5, where the Henry's law constant are plotted against the reciprocal of temperature (Shen et al., 2010, Ruthven, 1984, Yang, 1987).

Table 3: Virial model parameters fitting CO_2 and N_2 adsorption isotherms on Zeolite 13X at temperatures between 10 and 180 °C and pressures between 0 and 1.05 bar.

	K_∞	$-\Delta H$	A_0	A_1	B_0	B_1
	mol/(kg kPa)	kJ/mol	kg/mol	kg K/mol	kg^2/mol	kg^2 K/mol^2
CO_2	1.61935×10^{-7}	44.7838	0.4220	7.8371	−0.0485	34.8669
N_2	5.48207×10^{-7}	22.6591	−13.037	3889.5	24.9613	−7213.8

3.2. MBTSA process performances

Based on the CO_2 adsorption capacity at the feed gas conditions and the corresponding flow of CO_2 that is to be captured, it was possible to make an initial estimation of the amount of sorbent required (in terms of kg/s) and determine the size of the unit. Due to the large amount of flue gas to be processed (over 900 kg/s) it was necessary to employ two MBTSA units, as the gas velocity within the adsorption section must be kept below the minimum fluidization velocity and the size of the column should be limited to realistic values.

A set of simulations was then performed by varying several design parameters and operating conditions, as well as adjusting the system configuration, in order to reach the desired CO_2 purity and capture rate. Details on the system dimensions and operating conditions

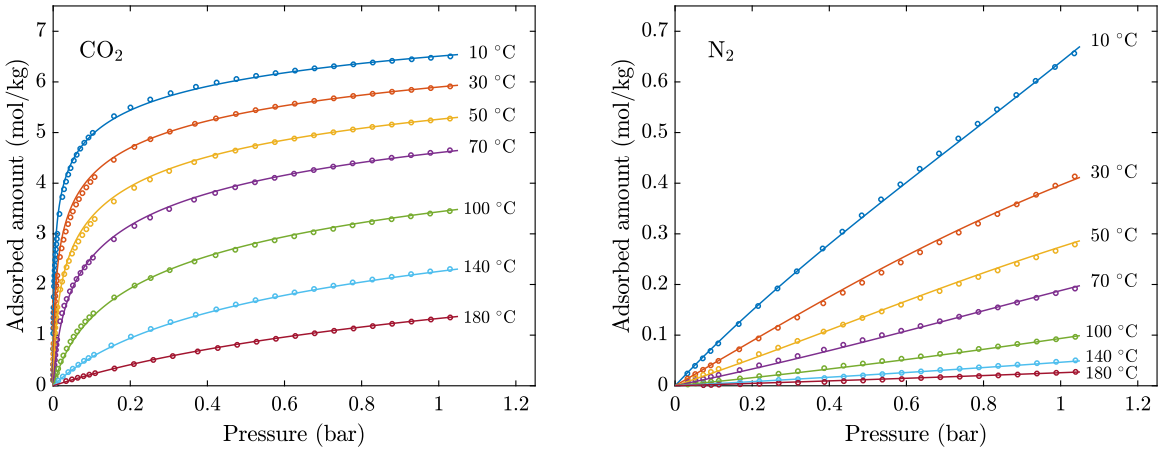

Figure 4: CO_2 (left) and N_2 (right) adsorption isotherms on Zeolite 13X at temperatures between 10 and 180 °C, and pressures up to 1.05 bar: experimental values (symbols) and fitting with Virial model (lines).

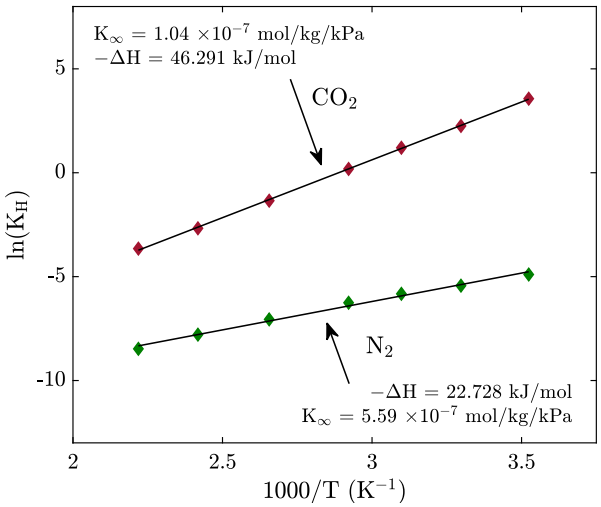

Figure 5: Van't Hoff plot for estimation of isosteric heat of adsorption: CO_2 in red and N_2 in green.

employed can be found in B.9. Results of the gPROMS simulations are shown in Figure 6 to Figure 9, in terms of N_2 and CO_2 concentration profiles reached at steady state in each section of the MBTSA. In all figures, the horizontal axis represents the position along the height (vertical coordinate) of the corresponding MBTSA section, being zero the bottom of the section, i.e. the sorbent outlet, while the upper limit of the axis corresponds to the top of the section. For clarity purpose, the flow directions of gas and sorbent are also shown on the plots, by the green arrows.

The corresponding temperature profiles, for both the gas and solid phases, are shown in Figure 10. In order to limit the increase in temperature due to the high heat of adsorption of CO_2, with a consequent reduction in adsorption capacity, it was decided to operate the

adsorption section similarly to the cooling section, where heat is removed from the sorbent by indirect heat exchange with cooling water. Nevertheless, an increase in temperature of nearly 20 °C is observed within the adsorption section.

Thanks to the high equilibrium selectivity of the Zeolite 13X, the adsorbent leaving the adsorption section contains a nearly negligible amount of N_2 in the adsorbed phase, which has a beneficial effect on the obtainable CO_2 purity. As it passes through the preheating section the CO_2 loaded adsorbent is heated from 30 °C to approximately 90 °C (solid outlet temperature). The change in temperature is accompanied by a change in CO_2/N_2 ratio in the gas phase (Figure 7), as part of the adsorbed CO_2 is released by the adsorbent. However, due to the high CO_2 adsorption capacity even at relatively high temperatures, the change in adsorbent loading taking place within the preheating section is very limited. This means that most of the desorption will take place in the desorption section, where the temperature is further increased to 180 °C (Case A) and 207 °C (Case B). In order to direct the gas flow towards the CO_2 extraction line, and thus avoiding upward gas flow within the desorption section, a mild vacuum (0.97 bar) is applied at the bottom of the section (sorbent outlet).

Due to the steepness of the CO_2 isotherm, when leaving the desorption section, the adsorbent loading of CO_2 is still significant (nearly 1 mol/kg). Part of this CO_2 can be removed from the adsorbent and recovered from the top of cooling section, by recirculating a small fraction of the CO_2-free gas from the adsorption section to the cooling section. If the flow or recirculated gas through the cooling section is sufficiently small, the gas leaving from the top will contain mostly CO_2 and can be mixed with the CO_2 product exiting the desorption section without excessively reducing the CO_2 purity.

The total amount of energy required for sorbent regeneration was evaluated by applying the energy balance across the preheating and desorption sections, where the adsorbent is heated to the regeneration temperature. The amount of thermal energy that can be recovered by transferring heat from the hot adsorbent leaving the desorption section to the adsorbent that has to be regenerated, was estimated by analyzing the temperature profiles along the heating and cooling sections, and the corresponding heat exchanged.

As expected, the system behavior is very sensitive to the regeneration temperature, as it directly affects the CO_2 working capacity and thus the amount of adsorbent required. A lower regeneration temperature, which is beneficial when considering heat integration using waste heat from the power plant, implies a less efficient regeneration of the sorbent and thus has to be compensated by increasing the amount of circulating sorbent. As an example of simulation results, two cases employing different regeneration temperatures are presented in Table 3. Better CO_2 purity and capture rate are obtained in the case of higher regeneration temperature (Case B), which also requires 16.3 % less adsorbent. When comparing the total amount of thermal energy required, the case using lower regeneration temperature (Case A) seems to be more efficient. However, due to the difference in CO_2 capture rate, the specific energy consumption of the two cases in terms of energy required per unit mass of CO_2 captured does not differ significantly.

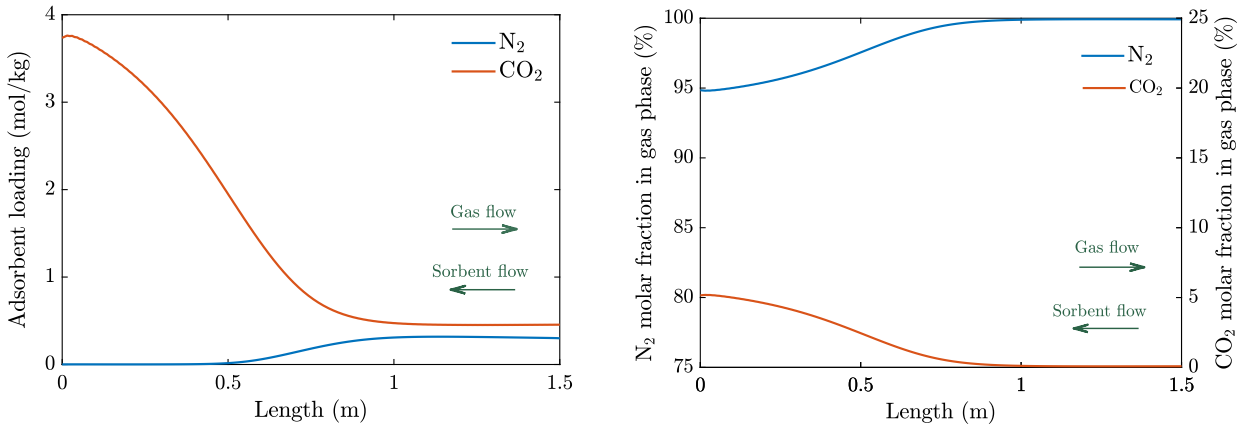

Figure 6: Adsorbent loading (left) and molar fraction (right) profiles along the vertical coordinate of the adsorption section.

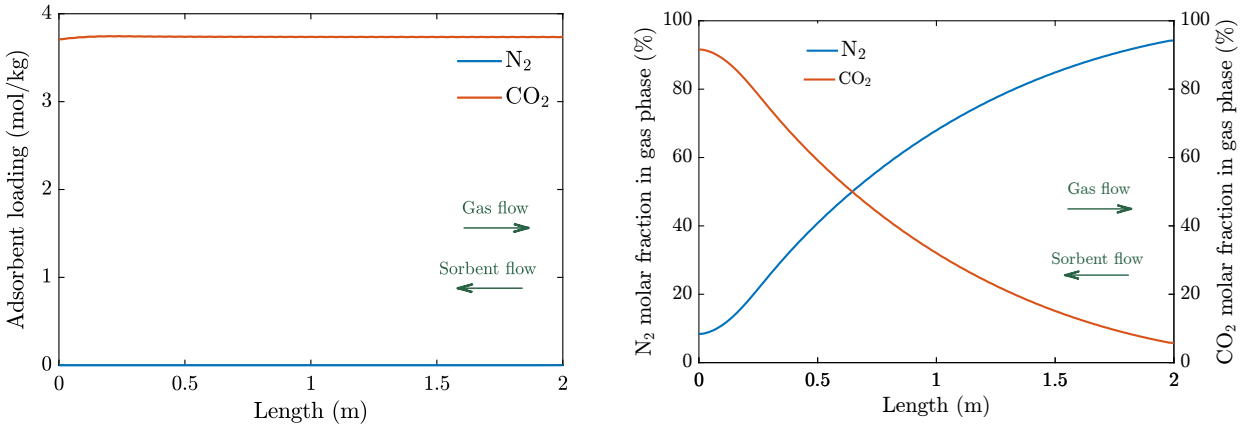

Figure 7: Adsorbent loading (left) and molar fraction (right) profiles along the vertical coordinate of the preheating section.

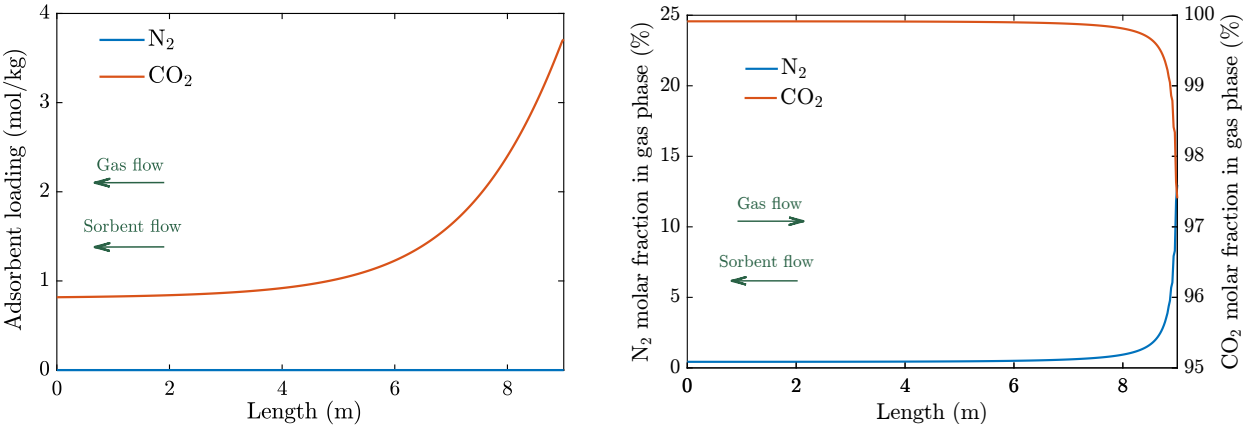

Figure 8: Adsorbent loading (left) and molar fraction (right) profiles along the vertical coordinate of the desorption section.

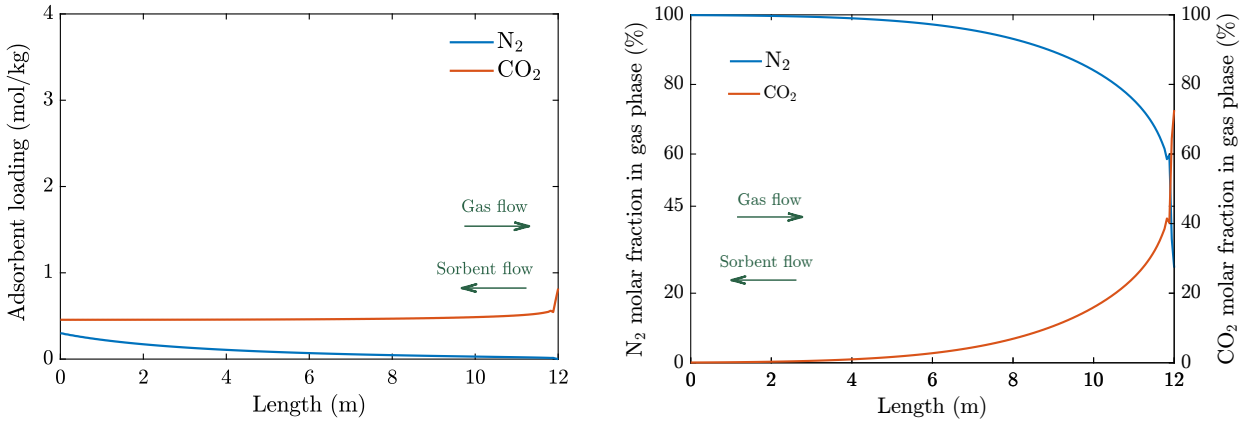

Figure 9: Adsorbent loading (left) and molar fraction (right) profiles along the vertical coordinate of the cooling section.

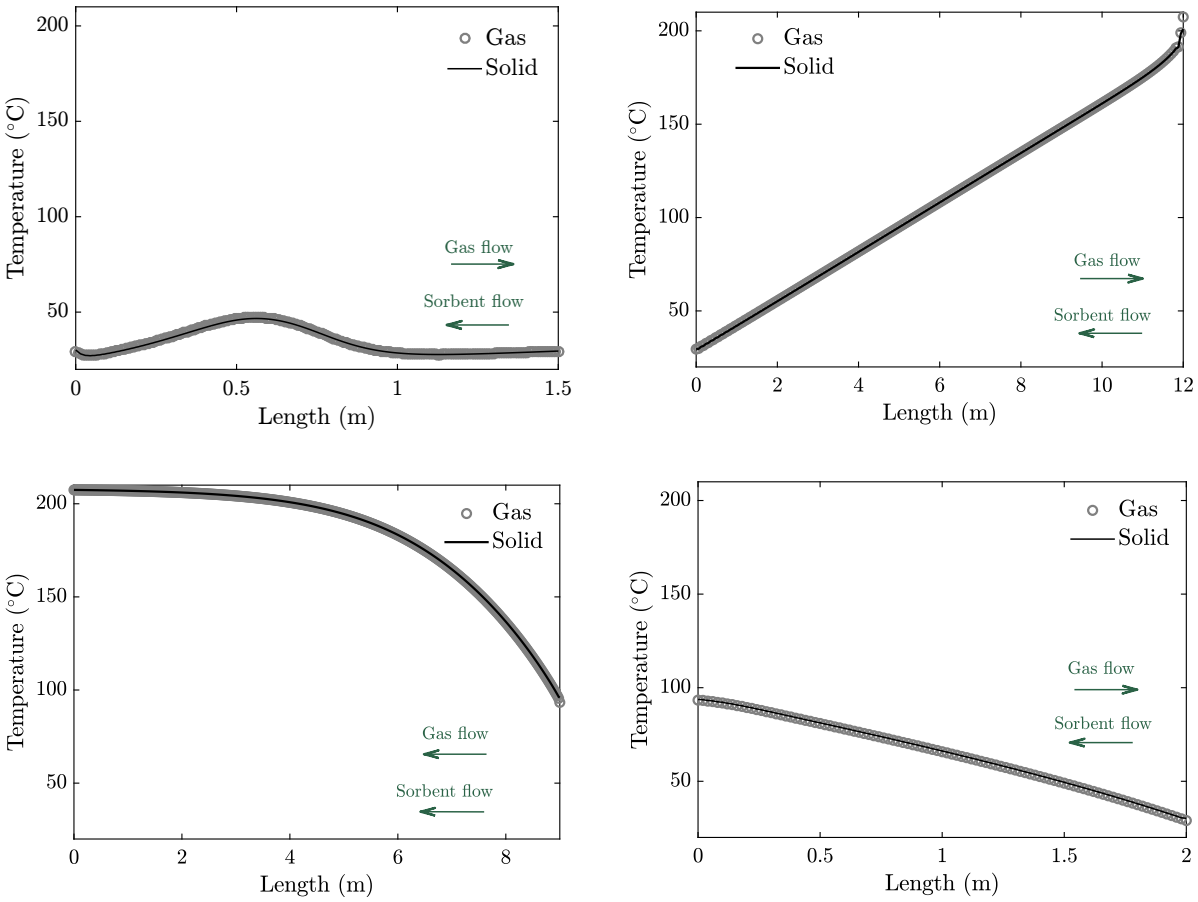

Figure 10: Temperature profiles along the vertical coordinate of: adsorption section (top left), cooling section (top right), desorption section (bottom left), cooling section (bottom right).

Table 4: Summary of process design and process simulation results for two case studies (values referred to the two MBTSA units).

	Case A	Case B
Amount of circulating sorbent	570 kg/s	490 kg/s
CO_2 working capacity	2.76 mol/$kg_{sorbent}$	3.28 mol/$kg_{sorbent}$
Regeneration temperature	180 °C	207 °C
CO_2 purity (%)	95.1	95.8
CO_2 capture rate (%)	96.0	98.2
Energy required for sorbent regeneration:		
- without heat integration	152.7 MW_{th}	158.7 MW_{th}
- with heat integration	101.2 MW_{th}	100.7 MW_{th}
Specific energy for sorbent regeneration:		
- without heat integration	2.21 MJ/$kg_{CO_2captured}$	2.24 MJ/$kg_{CO_2captured}$
- with heat integration	1.46 MJ/$kg_{CO_2captured}$	1.42 MJ/$kg_{CO_2captured}$

3.3. Results of the power plant integration

The main results of the Thermoflex (Thermoflow Version 27) simulations are shown in Table 3.3, where the following five cases are presented: (i) the NGCC without CO_2 capture as reference case, (ii) the NGCC coupled with a MEA capture process characterized by 90 % capture rate (which corresponds to the minimum target process specification), (iii) the NGCC coupled with a MEA capture process with a 95 % capture rate, for comparison purposes with the MBTSA system, (iv) the NGCC integrated with the MBTSA case using 180 °C as regeneration temperature (previously referred as Case A), (v) the NGCC integrated with the MBTSA case using 207 °C as regeneration temperature (previously referred as Case B). By comparing the investigated cases, the table shows how the different capture systems affect the power plant performance in terms of net electric efficiency, including a detailed list of the energy use associated to the capture process and power plant auxiliaries.

While the gas cycle is not affected by the capture process, as its operating conditions remain unchanged, the steam cycle suffers from a reduction in power generated, due to the steam bleeding for meeting the heat demand of the capture process. As regard to the MEA cases, low pressure steam is sufficient to provide the required heat, as the reboiler is operated at relatively low temperature (134 °C steam inlet temperature). On the contrary, the MBTSA process requires higher steam extraction pressures, depending on the sorbent regeneration temperature, in order to maintain the minimum pinch point within the heat exchanger. Although the MEA process requires steam at lower pressure, which is beneficial for the steam cycle performances, the total amount of heat to be provided by the steam is 2.5 times higher than for the MBTSA process. The overall reduction in power output due to steam bleeding is smaller when MBTSA process is chosen over the MEA process, confirming that the thermal energy requirement for regeneration is a crucial process parameters to consider when selecting a capture technology (Fernandez et al., 2014). However, when comparing the net electric efficiency of the power plant, no significant difference is observed between the two technologies, causing a reduction of about 7 and 8 percentage points for

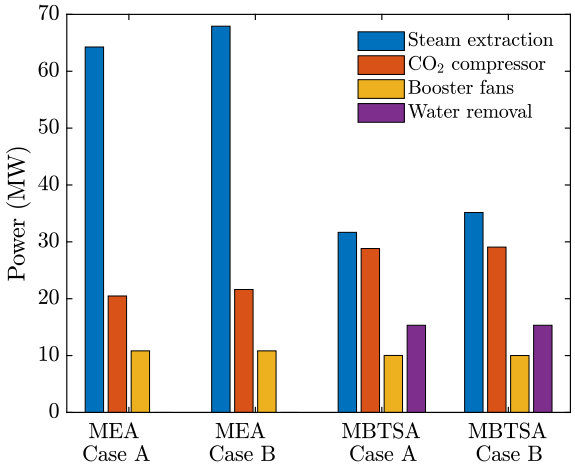

Figure 11: Individual contribution to the overall duty of the analyzed capture processes

the MBTSA and the MEA respectively. The reason for this is the higher energy required by MBTSA when comparing the CO_2 capture auxiliaries. In this respect, the higher energy consumption of the MBTSA are associated mainly to: (i) the use of the electric chiller for water removal, (ii) the CO_2 compressor, which uses approximately double amount of energy compared to the MEA case, due to the lower inlet pressure of the CO_2 to be compressed and the higher inlet temperature (180 °C, against 40 °C for the MEA process). A graphical representation of how the individual factors contribute to the total reduction in the net electric efficiency for each case is shown in Figure 11, where the power loss due to steam extraction is calculated as the difference between the steam turbine power output in the reference NGCC without CO_2 capture and the NGCC with the corresponding capture system.

In terms of net electric efficiency, the values obtained for the MEA process are in line with the results of similar studies available in literature (Lillia et al., 2018, Fernandez et al., 2014). Sanchez Fernandez et al.(Fernandez et al., 2014) estimated a 8.4 percentage points reduction, versus the 8.0 and 8.4 of this study, corresponding to Case A and Case B respectively. As expected, the higher energy penalty is associated to the MEA process with the higher capture rate (Case B). By increasing the capture rate, the heat input of the extracted steam also increases, with a negative effect on the power output.

With respect to the MBTSA processes, better performances in terms of net electric efficiency are obtained for Case A, in which the steam extracting pressure is lower, with a beneficial effect on the power output of the steam turbines. Despite the worse performance in term of net electric efficiency, Case B of MBTSA process outperform the other four cases evaluated in regards to the amount of CO_2 emitted by the power plant.

4. Conclusions

The application of MBTSA technology for CO_2 capture from a NGCC power plant is evaluated. The performances of the MBTSA process in terms of CO_2 capture rate and CO_2

Table 5: Results of the power plant integration with the MBTSA and comparison with the MEA capture process.

	without capture	MEA Case A	MEA Case B	MBTSA Case A	MBTSA Case B
Capture efficiency (%)	-	90.0	95.0	96.0	98.2
CO_2 captured (t/h)	-	229.4	242.2	243.2	248.8
CO_2 emitted (t/h)	253.4	23.9	11.2	10.1	4.6
Specific emissions (kg/MWh)	316.0	32.5	15.3	13.2	6.0
GT gross electric power output (MW)	555.3	555.3	555.3	555.3	555.3
ST gross electric power output (MW)	246.5	182.2	178.5	214.8	211.3
Gross power output (MW)	801.8	737.5	733.9	770.1	766.7
Net power output (MW)	792.7	693.1	688.1	692.9	689.0
Net electric efficiency (% LHV)	63.1	55.1	54.7	56.2	55.9
Details on the steam extraction:					
Steam extraction temperature (°C)		292	292	395	465
Steam extraction pressure (bar)		3.62	3.62	8.17	13.16
Steam extracted flow (kg/s)		106.8	101.2	38.0	35.9
Heat input (MW)		251.7	265.7	101.2	100.7
Detailed plant auxiliaries:					
Gas turbine auxiliaries (MW)	1.071	1.071	1.071	1.071	1.071
Condenser c.w. pump (MW)	0.728	0.423	0.384	0.559	0.569
Condensate forwarding pump (MW)	0.419	0.162	0.147	0.322	0.327
HP feedwater pump (MW)	4.604	4.609	4.609	4.605	4.605
IP feedwater pump (MW)	1.317	1.316	1.316	1.316	1.316
Steam turbine auxiliaries (MW)	0.518	0.383	0.375	0.451	0.444
Miscellaneous auxiliaries (MW)	0.401	0.369	0.367	0.385	0.383
Total CO_2 capture auxiliaries (MW)	0	36.090	37.459	54.493	54.728
Total plant auxiliaries (MW)	9.057	44.422	45.729	63.246	63.490
Detailed CO_2 capture auxiliaries:					
Booster fan(s) (MW)		10.827	10.827	10.023	10.008
Electric chiller (MW)				15.330	15.330
Intercooled compressor (MW)		20.479	21.617	28.824	29.077
Cooling water pump (MW)		2.165	2.252	0.316	0.315
Solvent circulation pump (MW)		1.973	2.082		
Condensate pump (MW)		0.014	0.015		
Others (MW)		0.632	0.667		

purity are assessed via dynamic simulations performed in gPROMS software. Input model parameters concerning the adsorbent material were provided by experimentally measuring adsorption isotherms on a pelletized sample of Zeolite 13X.

When designing the MBTSA process, two cases employing different regeneration temperatures (180 °C for Case A and 207 °C for Case B) were compared. In both cases the proposed system is able to meet the process target specifications, being the obtained CO_2 purity 95.1 % and 95.8 % for Case A and Case B respectively, with corresponding capture rates of 96.0% and 98.2 %.

Based on the performed MBTSA simulations, the thermal energy required for sorbent regeneration is estimated. Promising results are obtained when considering internal heat recovery, through which approximately 35 % of the total energy required can be saved.

A more comprehensive analysis of the energy consumption associated to the CO_2 capture process is performed by implementing a full plant model of the NGCC integrated with the capture process. The Thermoflex software is used for this purpose. Besides accounting for the effect of steam bleeding on the overall power plant performances, the developed model allows a detailed analysis of the energy penalties associated to the various CO_2 capture auxiliaries (e.g. booster fans, CO_2 compressor, and electric chiller for water removal from flue gas).

For comparison purposes, the application of a benchmark capture system was also considered, by suitably modifying the Thermoflex model of the reference NGCC. Interestingly, no significant difference is observed between the proposed MBTSA system and the MEA process: the overall net electric efficiency decreases from 63.1 % to 55.1 % and 56.2 % when applying the capture process to the MEA and the MBTSA respectively. While the MBTSA requires less steam when compared to the MEA system, the latter presents a lower energy penalty associated to the the CO_2 capture auxiliaries, compensating the higher effect associated to steam bleeding.

In conclusion, the results show that, based on the assumptions made, the simulated MBTSA process applied to NGCC power plant is suitable for capturing CO_2 at high purity and high capture rate, while being competitive with the state-of-the-art capture process in terms of energy penalties. Considering the much earlier stage of development of this technology in respect with the MEA process, the MBTSA seems to offer a larger potential for process improvement and should be considered for further development. In this respect, dedicated experimental activities are underway including testing of a lab scale MBTSA system.

Nomenclature

A	Virial isotherm model coefficients (kg mol^{-1})
a'	Particle specific area (m^2 m^{-3})
B	Virial isotherm model coefficients (kg^2 mol^{-1})
Bi	Biot number
$C_{p,g}$	Gas mixture mass specific heat at constant pressure (J kg^{-1} K^{-1})
c_p	Gas mixture molar specific heat at constant pressure (J mol^{-1} K^{-1})
$c_{p,pack}$	Specific heat capacity of packing material (J kg^{-1} K^{-1})
$c_{p,s}$	Specific heat capacity of the adsorbent (J kg^{-1} K^{-1})
c_v	Gas mixture molar specific heat at constant volume (J mol^{-1} K^{-1})
$C_{b,i}$	Molar concentration of component i in the macropores (mol m^{-3})
C_i	Molar concentration of component i (mol m^{-3})
C_T	Total gas concentration (mol m^{-3})
D_c	Micropore effective diffusivity of component i (m^2 s^{-1})
D_c^0	Micropore limiting diffusivity at infinite temperature (m^2 s^{-1})
D_{ij}	Binary molecular diffusivity (m^2 s^{-1})
D_h	Hydraulic diameter (m)
D_m	Molecular diffusivity (m^2 s^{-1})
$D_{p,i}$	Macropore diffusivity of component i (m^2 s^{-1})
D_z	Axial dispersion coefficient (m^2 s^{-1})
d_p	Particle diameter (m)
E_a	Activation energy of micropore diffusion (kJ mol^{-1})
k_g	Thermal conductivity of the gas (W m^{-1} K^{-1})
K_i	Equilibrium constant of component i
K_i^∞	Equilibrium constant at infinite temperature (mol kg^{-1} kPa^{-1})
h_f	Film heat transfer coefficient between the gas and the solid (J s^{-1} m^{-2} K^{-1})
$h_{g,hx}$	Film heat transfer coefficient between the gas and the wall (J s^{-1} m^{-2} K^{-1})
K_m	Film mass transfer coefficient (m s^{-1})
M_w	Molecular weight (g mol^{-1})
q_i	Adsorbed phase concentration of component i (mol kg^{-1})
R	Ideal gas constant (J K^{-1} mol^{-1})
r_c	Crystals radius (m)
R_p	Particle radius (m)
P_i	Partial pressure of component i (kPa)
T	Temperature of the gas (K)
T_s	Temperature of the solid (K)
T_hx	Temperature of the wall (K)
u	Superficial velocity of the gas (m s^{-1})
v_{solid}	Velocity of the solid (m s^{-1})
Y_i	Molar fraction of component i

Greek letters	
ΔH	Isosteric heat of adsorption (kJ mol^{-1})
ε	Bed void fraction
ε_p	Particle porosity
λ	Heat axial dispersion coefficient (J m^{-1} s^{-1} K^{-1})
μ_g	Gas viscosity (Pa s)
ξ	Packing porosity factor
ρ_g	Gas density (kg m^{-3})
ρ_p	Particle density (kg m^{-3})
ρ_{pack}	Packing density (kg m^{-3})
$\Omega_{D_{ij}}$	Dimensionless collision integral of binary diffusivity

Acknowledgments

We acknowledge the Research Council of Norway for its financial support through the EDemoTeC project (Grant no. 267873) within the CLIMIT program.

Appendix A. Fuel properties and MEA process specifications

Table A.6: Fuel specification used in the NGCC simulations

Volumetric composition		
Hydrogen	H_2	0.36 %
Oxygen	O_2	0.07 %
Nitrogen	N_2	3.65 %
Carbon monoxide	CO	0.09 %
Carbon dioxide	CO_2	0.34 %
Methane	CH_4	87 %
Ethane	C_2H_6	8.46 %
Ethylene	C_2H_6	0.03 %
Heating values		
LHV	46280	kJ/kg
HHV	51237	kJ/kg

Table A.7: Specification of the MEA capture process

Parameter	**Value**
Specific energy input (Fernandez et al., 2014)	3.95 MJ/kg
Cooler exit temperature	40 °C
CO_2 compressor inlet temperature	40 °C
CO_2 compressor inlet pressure	1.6 bar
CO_2 compressor delivery pressure	110 bar
Number of compressor stages	5
Booster fan isentropic efficiency	85 %
Booster fan mech.+ elec. efficiency	95 %
Pumps efficiency	75 %
Total gas pressure drop (in absorber)	0.1 bar
Steam pressure at reboiler inlet (Fernandez et al., 2014)	3.05 bar
Steam temperature at reboiler inlet (Fernandez et al., 2014)	134 °C

Appendix B. Main assumptions and remarks on the MBTSA model

The conservation equations describing the moving bed adsorption system are obtained by assuming that mass, velocity and temperature gradients in the radial direction are negligible. The model also assumes ideal gas behaviour in the bulk phase, constant cross sectional area, constant velocity of the adsorbent and constant void fraction.

In the resulting one-dimensional balance equations, detailed in Figure 2, two phases can be distinguished: (i) a gas phase, which exchanges energy and mass with the adsorbent, and only energy with the wall; and (ii) a solid phase, onto which the gas diffuses and adsorbs.

The main model variables are therefore: gas velocity and pressure, gas concentrations of each component in the bulk phase, gas concentrations in the macropores of the adsorbents, adsorbed phase concentrations, temperature of the bulk gas phase and temperature of the solid phase. While the pressure drops are computed using the Ergun equation, the adsorption equilibrium between the gas phase in the macropores and the adsorbed phase is described by the Virial isotherms model.

The adsorption kinetics is predicted with a lumped resistance model based on the Linear Driving Force (LDF) approximation. The exponential temperature dependence typical of activated processes is used to compute the effective diffusivity within the adsorbent. The model equation and parameters used for this purpose are given in Table B.8, together with other supplementary equations and correlations used in the simulations.

As previously mentioned, for providing (and removing) the necessary heat to the system, an indirect contact type heat exchanger configuration was assumed. For simplicity, a constant convective heat transfer parameter ($h_{g,hx}$), and fixed temperature of the heat transfer surface along the vertical axis (T_{hx}) were assumed. The hydraulic diameter (D_h) of the adsorbent-gas side (i.e. the ratio between the volume of the adsorbent-gas side and the heat transfer area on the same side, at a given positing along the vertical axis) is adjusted in order to ensure that sufficient heat transfer area is available, thus allowing the adsorbent

to reach the desired temperature within the traversed heat exchanger. Numerical values of the assumed heat transfer parameters, system dimensions, and residence times within each sections of the moving bed are given in Table B.9.

Table B.8: Supplementary equations and model parameters used in the MBTSA simulations

Correlations	
Molecular diffusivity (Wilke, 1950)	$D_m = \frac{1-y_i}{\sum_{j\neq i}^{n} \frac{y_i}{D_{ij}}}$
Binary diffusivity (Bird et al., 2002)	$D_{ij} = \frac{0.01883\ T^{3/2}}{P\ \sigma_{ij}^2\ \Omega_{D_{ij}}} \sqrt{\frac{1}{M_{w,i}} + \frac{1}{M_{w,j}}}$
Macropore diffusivity (Yang, 1987)	$\frac{1}{D_p} = \tau_p \left(\frac{1}{D_k} + \frac{1}{D_m} \right)$
Knudsen diffusivity (Ruthven, 1984)	$D_k = 97\ r_p \sqrt{\frac{T}{M_w}}$
Rate of adsorption in micropores	$\frac{D_c}{r_c^2} = \frac{D_c^0}{r_c^2} \exp\left(\frac{E_a}{RT}\right)$
Axial dispersion coefficient	$D_z = \frac{D_m}{\varepsilon_c}(20 + 0.5\ \mathrm{Sc}\ \mathrm{Re})$
Axial thermal conductivity of gas	$\lambda = k_g\,(7 + 0.5\ Pr\ Re)$
Scherwood number correlation	$\mathrm{Sh} = 2.0 + 1.1\ \mathrm{Re}^{0.6}\ \mathrm{Sc}^{1/3}$
Nusselt number correlation	$\mathrm{Nu} = 2.0 + 1.1\mathrm{Re}^{0.6}\ \mathrm{Pr}^{1/3}$
Dimensionless numbers	**Parameters value**
Biot Bi= $\frac{r_p k_f}{\varepsilon_p D_p}$	Bed void fraction (ads. section): $\varepsilon_c = 0.8$
Reynolds Re= $\frac{\rho_g u d_p}{\mu_g}$	Bed void fraction (other sections): $\varepsilon_c = 0.6$
Schmidt Sc= $\frac{\mu_g}{\rho_g D_m}$	Parameters of adsorption rate:
Prandtl Pr= $\frac{C_{p,g}\mu_g}{k_g}$	CO_2: $E_a = 15$ kJ/mol; $D_c^0/r^2 = 25\ \mathrm{s}^{-1}$
Sherwood Sh= $\frac{k_f d_p}{D_m}$	N_2: $E_a = 12$ kJ/mol; $D_c^0/r^2 = 10\ \mathrm{s}^{-1}$

Table B.9: Details on the MBTSA design and parameters

	MBTSA section			
	Adsorption	Preheating	Desorption	Cooling
Length (m)	1.5	2	9	12
Number of discretization intervals	200	100	400	200
Inlet gas superficial velocity (m s^{-1})	1.50			
Cross sectional area (m^2)	254.5	78.5	78.5	78.5
Adsorbent residence time (s)	257	247	1111	1481
Heat transfer coefficient (W m^{-2} s^{-1})	90	90	90	90
Hydraulic diameter (m)	0.04	0.10	0.10	0.08

References

Anantharaman, R., Bolland, O., Booth, N., van Dorst, E., Ekstrom, C., Fernandez, E.S., Editor, F.F., Macchi, E., Manzolini, G., Nikolic, D., Pfeffer, A., Prins, M., Rezvani, S., Robinson, L., 2011. CESAR-D2.4.3-APPROVED-European Best Practice Guidelines for CO_2 Capture Technologies - EBTF. Technical Report. Alstom UK, NTNU, E.ON, Shell, Vattenfall, TNO, Alstom UK, Polit. di Milano, Univ. of Ulster.

Baksh, M.S.A., Kikkinides, E.S., Yang, R.T., 1992. Lithium type X zeolite as a superior sorbent for air separation. Separation Science and Technology 27, 277–294.

Barrer, R.M., 1981. Sorption in porous crystals: equilibria and their interpretation. Journal of Chemical Technology and Biotechnology 31, 71–85.

Bird, R.B., Stewart, W.E., Lightfoot, E.N., 2002. Transport Phenomena. Second Edition. Wiley, New York.

Chue, K., Kim, J., Yoo, Y., Cho, S., Yang, R., 1995. Comparison of activated carbon and zeolite 13X for CO_2 recovery from flue gas by pressure swing adsorption. Industrial and Research, Engineering Chemistry 34, 591–598.

Fernandez, E.S., Goetheer, E., Manzolini, G., Macchi, E., Rezvani, S., Vlugt, T., 2014. Thermodynamic assessment of amine based CO_2 capture technologies in power plants based on european benchmarking task force methodology. Fuel 129, 318 – 329.

Franco, F., Anantharaman, R., Bolland, O., Booth, N., van Dorst, E., Ekstrom, C., Fernandes, E., Macchi, E., Manzolini, G., Nicolic, D., Pfeffer, A., Prins, M., Rezvani, S., Robinson, L., 2011. Test Cases and Preliminary Benchmarking Results from the Three Projects. Technical Report. Alstom UK.

gPROMS Model Builder Version 5.0, 2016. Process System Enterpise (PSE). UK.

Grande, C.A., Kvamsdal, H., Mondino, G., Blom, R., 2017. Development of moving bed temperature swing adsorption (MBTSA) process for post-combustion CO_2 capture: Initial benchmarking in a (NGCC) context. Energy Procedia 114, 2203–2210.

Hefti, M., Marx, D., Joss, L., Mazzotti, M., 2015. Adsorption equilibrium of binary mixtures of carbon dioxide and nitrogen on zeolites ZSM-5 and 13X. Microporous and Mesoporous Materials 215, 215–228.

Hornbostel, M.D., Bao, J., Krishnan, G., Nagar, A., Jayaweera, I., Kobayashi, T., Sanjurjo, A., Sweeney, J., Carruthers, D., Petruska, M.A., 2013. Characteristics of an advanced carbon sorbent for CO_2 capture. Carbon 56, 77–85.

Kim, K., Park, Y.K., Park, J., Jung, E., Seo, H., Kim, H., Lee, K.S., 2014. Performance comparison of moving and fluidized bed sorption systems for an energy-efficient solid sorbent-based carbon capture process. Energy Procedia 63, 1151–1161.

Kim, K., Son, Y., Lee, W.B., Lee, K.S., 2013. Moving bed adsorption process with internal heat integration for carbon dioxide capture. International Journal of Greenhouse Gas Control 17, 13–24.

Knaebel, K., 2009. Temperature swing adsorption system.

Liang, Z., Fu, K., Idem, R., Tontiwachwuthikul, P., 2016. Review on current advances, future challenges and consideration issues for post-combustion co_2 capture using amine-based absorbents. Chinese Journal of Chemical Engineering 24, 278–288.

Lillia, S., Bonalumi, D., Grande, C., Manzolini, G., 2018. A comprehensive modeling of the hybrid temperature electric swing adsorption process for CO_2 capture. International Journal of Greenhouse Gas Control 74, 155–173.

Liu, Z., Grande, C.A., Li, P., Yu, J., Rodrigues, A.E., 2011. Multi-bed vacuum pressure swing adsorption for carbon dioxide capture from flue gas. Separation and Purification Technology 81, 307–317.

Merel, J., Clausse, M., Meunier, F., 2008. Experimental investigation on CO_2 post-combustion capture by indirect thermal swing adsorption using 13X and 5A zeolites. Industrial & Engineering Chemistry Research 47, 209–215.

Mondino, G., Grande, C.A., Blom, R., 2017. Effect of gas recycling on the performance of a moving bed temperature-swing (MBTSA) process for CO_2 capture in a coal fired power plant context. Energies 10, 745.

Park, Y.J., Lee, S.J., Moon, J.H., Choi, D.K., Lee, C.H., 2006. Adsorption equilibria of O_2, N_2, and Ar on carbon molecular sieve and zeolites 10X, 13X, and LiX. Journal of Chemical and Data, Engineering 51, 1001–1008.

Plaza, M.G., Rubiera, F., Pevida, C., 2017. Evaluating the feasibility of a TSA process based on steam stripping in combination with structured carbon adsorbents to capture CO_2 from a coal power plant. Energy & Fuels 31, 9760–9775.

Ribeiro, A.M., Sauer, T.P., Grande, C.A., Moreira, R.F.P.M., Loureiro, J.M., Rodrigues, A.E., 2008. Adsorption equilibrium and kinetics of water vapor on different adsorbents. Ind. Eng. Chem. Res 47, 7019–7026.

Ruthven, D.M., 1984. Principles of adsorption and adsorption processes. John Wiley & Sons.

Shen, C., Grande, C.A., Li, P., Yu, J., Rodrigues, A.E., 2010. Adsorption equilibria and kinetics of CO_2 and N_2 on activated carbon beads. Chemical Engineering Journal 160, 398–407.

Shen, C., Liu, Z., Li, P., Yu, J., 2012. Two-Stage VPSA process for CO_2 Capture from Flue Gas Using Activated carbon beads. Industrial & Engineering Chemistry Research 51, 5011–5021.

Son, Y., Kim, K., Lee, K.S., 2014. Feasibility study of a moving-bed adsorption process with heat integration for CO_2 capture through energy evaluation and optimization. Energy & Fuels 28, 7599–7608.

Taqvi, S.M., LeVan, M.D., 1997. Virial description of two-component adsorption on homogeneous and heterogeneous surfaces. Industrial & Engineering Chemistry Research 36, 2197–2206.

Thermoflow Version 27, 2017. Termoflow Inc.

Vandervort, C., 2018. Advancements in H class gas turbines and combined cycle power plants, in: ASME Turbo Expo 2018: Turbomachinery Technical Conference and Exposition, American Society of Mechanical Engineers. pp. V003T08A007–V003T08A007.

Wilke, C.R., 1950. Diffusional properties of multicomponent gases. Chemical Engineering Progress 46, 95–104.

Yang, R.T., 1987. Gas separation by adsorption processes. Butterworth-Heinemann.

Zanco, S.E., Mazzotti, M., Gazzani, M., Romano, M.C., Martínez, I., 2018. Modeling of circulating fluidized beds systems for post-combustion CO_2 capture via temperature swing adsorption. AIChE Journal 64, 1744–1759.